COMPDYN 2013
4th ECCOMAS Thematic Conference on
Computational Methods in Structural Dynamics and Earthquake Engineering
M. Papadrakakis, N.D.Lagaros, V. Plevris (eds.)
Kos Island, Greece, 12–14 June 2013

A NONLINEAR VEHICLE-STRUCTURE INTERACTION METHODOLOGY WITH WHEEL-RAIL DETACHMENT AND REATTACHMENT

P. A. Montenegro[1], S.G.M. Neves[2], A.F.M. Azevedo[4] and R. Calçada[3]

[1,2,3,4] University of Porto, Faculty of Engineering
Rua Dr. Roberto Frias s/n, 4200-465 Porto, Portugal

[2] Polytechnic Institute of Porto, ISEP
Rua Dr. António Bernardino de Almeida, 431, 4200-072 Porto, Portugal

[1] pedro.montenegro@fe.up.pt
[2] sgm.neves@fe.up.pt
[3] alvaro@fe.up.pt
[4] ruiabc@fe.up.pt

Keywords: Vehicle-Structure Interaction, Dynamic Analysis, Nonlinear Contact, Lagrange Multipliers, Bridge.

Abstract. *A vehicle-structure interaction methodology with a nonlinear contact formulation based on contact and target elements has been developed. To solve the dynamic equations of motion, an incremental formulation has been used due to the nonlinear nature of the contact mechanics, while a procedure based on the Lagrange multiplier method imposes the contact constraint equations when contact occurs. The system of nonlinear equations is solved by an efficient block factorization solver that reorders the system matrix and isolates the nonlinear terms that belong to the contact elements or to other nonlinear elements that may be incorporated in the model. Such procedure avoids multiple unnecessary factorizations of the linear terms during each Newton iteration, making the formulation efficient and computationally attractive. A numerical example has been carried out to validate the accuracy and efficiency of the present methodology. The obtained results have shown a good agreement with the results obtained with the commercial finite element software ANSYS.*

1 INTRODUCTION

The dynamic interaction between vehicles and structure has attracted much attention during the last three decades due to the increase of the loads and speed of the vehicles. Such factors strongly influence the interaction between both systems. In the particular case of railways, the maintenance of the existing high-speed rail networks and the construction of new lines urge the development of new algorithms that can accurately and efficiently analyze the interaction between both systems.

With the increase of the running speed, the probability of incidents such has track instability or derailments also increases. Therefore, the development of more complex train-bridge interaction models that can accurately evaluate the train running safety is a major topic of research.

A significant number of studies have been conducted in the last decades to better understand this phenomenon. In a problem of this type, the model has to guarantee the coupling between the independent systems by establishing the dynamic equilibrium through two sets of equations of motion, one for the vehicle and one for the structure. One way to solve these equations is through an iterative procedure which ensures the coupling between the two systems [1-3]. Such methods, despite being simpler to implement, may require a large computational effort and can lead to convergence problems.

Yang et al. [4] proposed another approach to solve the coupled equations which consisted on condensing the degrees of freedom (d.o.f.) of the vehicle to those of the bridge elements in contact. With such approach, the system matrix is time-dependent and has to be factorized at each time step.

Most finite element programs are able to handle contact problems using either the penalty method or the Lagrange Multiplier method [5]. However, these methods are mostly used in multibody dynamic simulations that do not take into account the track flexibility [6-7]. Antolin et al. [8] proposed an hybrid finite element/multibody formulation that used the penalty method to introduce geometrical constraints in the equilibrium equations. These constraints are formulated based on lookup tables that establish the geometrical compatibility between the wheels and rails. Unlike other multibody formulations, this approach takes into consideration the flexibility of the track and structure, but cannot deal with situations where the wheel and rail lose contact.

Tanabe et al. [9] developed a train-structure interaction software, DIASTARS, in which the train is modeled as a multibody system, while the bridge is modeled with finite elements to take the structure flexibility into account. This methodology divides the wheel-rail contact in two modes, one vertical and one lateral, that are simulated with nonlinear contact springs to represent the wheel-rail contact stiffness. Hence, no specific contact methods are used in this approach.

Neves et al. [10] developed a simple methodology based on the Lagrange multipliers method in which the dynamic equilibrium equations of both systems are complemented with additional displacement compatibility equations, forming a single system of equations that can be directly solved. However, this method did not take into account the nonlinearities presented in a wheel-rail contact problem such as the bodies separation or deformations.

In the present paper, a contact search algorithm based on contact and target elements is used to detect which elements are in contact. When contact occurs, contact constraints equations are imposed using a procedure based on the Lagrange multipliers method, while the dynamic equations of motion are solved through an incremental formulation due to the nonlinear nature of the contact mechanics. These two types of nonlinear equations form a single system with displacements and contact forces as unknowns. In order to solve the problem efficiently,

a block factorization solver that reorders the system matrix is also presented. This solver avoids multiple factorizations of the linear terms during each Newton iteration, making the formulation computationally attractive

The proposed methodology is referred to as the direct method and has been implemented in MATLAB [11] which import and manipulate the structural matrices extracted from ANSYS [12], a commercial finite element software used to model the vehicle and structure. A numerical example is presented to evaluate the efficiency and accuracy of the proposed vehicle-structure interaction methodology.

2 GENERAL CONCEPT OF THE ALGORITHM

2.1 Contact algorithm concept

The vehicle-structure interaction problem can be solved by a direct method [10], based on the Lagrange multiplier method, that avoids an iterative procedure to ensure the coupling between the two systems. This method complements the dynamic equilibrium equations of both systems with additional constraint equations, forming a single system of equations that can be directly and efficiently solved. However, when the contact nonlinearities are taken into account an iterative algorithm has to be added to the formulation in order to solve the nonlinear equations. The iterative schemes most widely used for the solution of nonlinear finite element equations are based on the Newton method [13-14].

When studying the contact between two bodies, the surface of one body is conventionally taken as a contact surface and the surface of the other body as a target surface (see Figure 1). This contact pair concept is widely used in computational contact mechanics. A two-dimensional node-to-segment contact element is used in the present paper but the extension of the formulation to other types of finite elements and to three-dimensional problems is straightforward. The algorithm used does not account for the surface profiles of the contact and target elements.

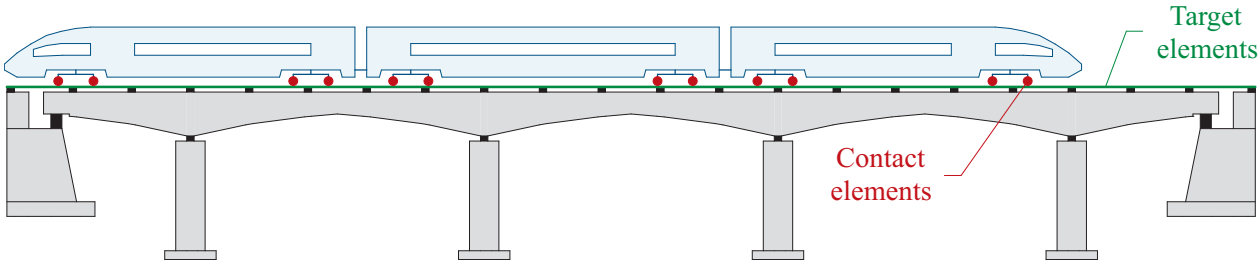

Figure 1: Contact pair concept.

In the present paper, a contact search algorithm is used to detect which elements are in contact, being the contact constraints only imposed when contact occurs. Since only the frictionless contact is considered herein, the contact constraint equations are purely geometrical constraints that relate the displacements of the contact node to the displacements of the corresponding target element.

2.2 Classification of the degrees of freedom

Since the main nonlinearities of the system are concentrated on the d.o.f. of the contact elements, the corresponding terms of these elements in the system matrix can be reordered and manipulated to avoid multiple factorizations of the entire matrix in each Newton iteration (see section 4). This procedure is also valid for other nonlinear elements, such as nonlinear sus-

pension in the vehicles or nonlinear bearings in the structure. Table 1 shows the d.o.f. classification adopted in the present algorithm.

I	Unconstrained nodal d.o.f. (linear terms)
R	Reordered nodal d.o.f. (nonlinear terms)
Y	Contact nodal d.o.f.
F	Free nodal d.o.f. (includes *I*, *R* and *Y* type d.o.f.)
P	Prescribed nodal d.o.f.

Table 1: Classification of the d.o.f.

The *I* type d.o.f. correspond to all unconstrained d.o.f. without any nonlinear property, the *R* type d.o.f. correspond to the nonlinear terms that are reordered for efficiency (material nonlinearities), *Y* type d.o.f. correspond to the nonlinear terms from the contact elements and the *P* type d.o.f. are the prescribed d.o.f. Note that, despite both *R* and *Y* type d.o.f. correspond to the same type of d.o.f. (nonlinear unconstrained d.o.f.), the algorithm separate them, since the dimension of the *Y* type d.o.f. can vary due to the changes of the contact status (the *Y* type d.o.f. exists only if contact occurs). The above mentioned d.o.f. classification is illustrated in Figure 2.

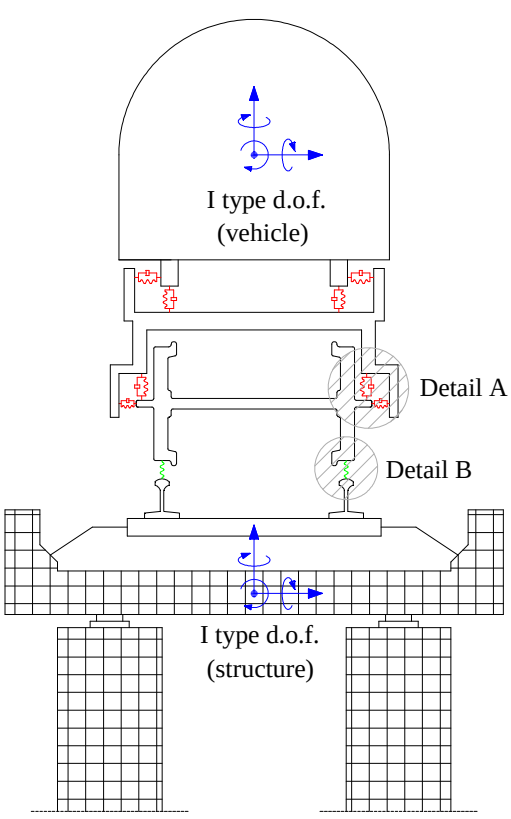

a) Vehicle-structure interaction scheme

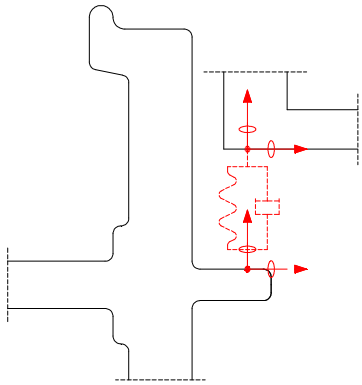

b) Detail A - *R* type d.o.f. in a nonlinear suspension

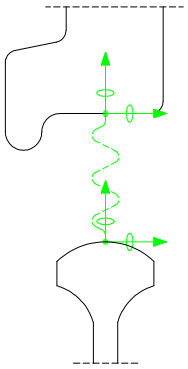

c) Detail B - *Y* type d.o.f. in the contact element

Figure 2: Schematic representation of the d.o.f. classification

3 VEHICLE-STRUCTURE INTERACTION FORMULATION

3.1 Formulation of the nonlinear dynamic equations

In a nonlinear dynamic analysis, the nodal point forces corresponding to the internal element stresses may depend nonlinearly on the nodal point displacements [13]. Based on the

α method [15] and assuming that the applied loads are deformation-independent, the equations of motion of the vehicle-structure system can be expressed as

$$\mathbf{M}\,\ddot{\mathbf{a}}^{c} + \mathbf{C}\left[(1+\alpha)\,\dot{\mathbf{a}}^{c} - \alpha\,\dot{\mathbf{a}}^{p}\right] + (1+\alpha)\,\mathbf{R}^{c} - \alpha\,\mathbf{R}^{p} = (1+\alpha)\,\mathbf{F}^{c} - \alpha\,\mathbf{F}^{p} \tag{1}$$

where **M** is the mass matrix, **C** is the viscous damping matrix, **R** is nodal point forces corresponding to the internal element stresses, **F** is the externally applied nodal loads vector and **a** are the nodal displacements. The superscript *c* indicates the current time step ($t + \Delta t$) and the superscript *p* indicates the previous one (t).

To solve Eq. (1) let the *F* type d.o.f. represent the free nodal d.o.f., whose values are unknown, and the *P* type d.o.f. represent the prescribed nodal d.o.f., whose values are known. Thus, the load vector can be expressed as

$$\mathbf{F}_{F} = \mathbf{P}_{F} + \mathbf{D}_{FX}^{CE}\ \mathbf{X}^{CE} + \mathbf{D}_{FX}^{TE}\ \mathbf{X}^{TE} \tag{2}$$

$$\mathbf{F}_{P} = \mathbf{P}_{P} + \mathbf{D}_{PX}^{CE}\ \mathbf{X}^{CE} + \mathbf{D}_{PX}^{TE}\ \mathbf{X}^{TE} + \mathbf{S} \tag{3}$$

where **P** corresponds to the externally applied nodal loads whose values are known and **S** are the support reactions. The matrices **D** relate the contact forces defined in the local coordinate system of each contact pair to the nodal point forces in the global coordinate system. The superscripts *CE* and *TE* denote contact and target element respectively.

The equilibrium between the two bodies is guaranteed only if the forces acting in the contact interface respect the following equation

$$\mathbf{X}^{CE} + \mathbf{X}^{TE} = 0 \tag{4}$$

Thus, Substituting Eq. (4) into Eqs. (2) and (3) leads to

$$\mathbf{F}_{F} = \mathbf{P}_{F} + \mathbf{D}_{FX}\ \mathbf{X} \tag{5}$$

$$\mathbf{F}_{P} = \mathbf{P}_{P} + \mathbf{D}_{PX}\ \mathbf{X} + \mathbf{S} \tag{6}$$

where

$$\mathbf{X} = \mathbf{X}^{CE} \tag{7}$$

$$\mathbf{D}_{FX} = \mathbf{D}_{FX}^{CE} - \mathbf{D}_{FX}^{TE} \tag{8}$$

$$\mathbf{D}_{PX} = \mathbf{D}_{PX}^{CE} - \mathbf{D}_{PX}^{TE} \tag{9}$$

Substituting Eqs. (5) and (6) into Eq. (1) and partitioning into *F* and *P* type d.o.f. gives

$$\begin{bmatrix} \mathbf{M}_{FF} & \mathbf{M}_{FP} \\ \mathbf{M}_{PF} & \mathbf{M}_{PP} \end{bmatrix} \begin{bmatrix} \ddot{\mathbf{a}}_{F}^{c} \\ \ddot{\mathbf{a}}_{P}^{c} \end{bmatrix} + \begin{bmatrix} \mathbf{C}_{FF} & \mathbf{C}_{FP} \\ \mathbf{C}_{PF} & \mathbf{C}_{PP} \end{bmatrix} \left[(1+\alpha) \begin{bmatrix} \dot{\mathbf{a}}_{F}^{c} \\ \dot{\mathbf{a}}_{P}^{c} \end{bmatrix} - \alpha \begin{bmatrix} \dot{\mathbf{a}}_{F}^{p} \\ \dot{\mathbf{a}}_{P}^{p} \end{bmatrix} \right] + (1+\alpha) \begin{bmatrix} \mathbf{R}_{F}^{c} \\ \mathbf{R}_{P}^{c} \end{bmatrix} - \alpha \begin{bmatrix} \mathbf{R}_{F}^{p} \\ \mathbf{R}_{P}^{p} \end{bmatrix}$$
$$= (1+\alpha) \begin{bmatrix} \mathbf{P}_{F}^{c} + \mathbf{D}_{FX}\ \mathbf{X}^{c} \\ \mathbf{P}_{P}^{c} + \mathbf{D}_{PX}\ \mathbf{X}^{c} + \mathbf{S}^{c} \end{bmatrix} - \alpha \begin{bmatrix} \mathbf{P}_{F}^{p} + \mathbf{D}_{FX}\ \mathbf{X}^{p} \\ \mathbf{P}_{P}^{p} + \mathbf{D}_{PX}\ \mathbf{X}^{p} + \mathbf{S}^{p} \end{bmatrix} \tag{10}$$

The first line of blocks in Eq. (10) represents the system of nonlinear equations that has to be solved in order to calculate the unknowns of the problem (displacements and contact forces). Rearranging the first line of blocks leads to

$$\mathbf{M}_{FF}\,\ddot{\mathbf{a}}_{F}^{c} + (1+\alpha)\mathbf{C}_{FF}\,\dot{\mathbf{a}}_{F}^{c} + (1+\alpha)\mathbf{R}_{F}^{c} - (1+\alpha)\,\mathbf{D}_{FX}\ \mathbf{X}^{c} = \overline{\mathbf{F}}_{F} \tag{11}$$

where

$$\begin{aligned}\overline{\mathbf{F}}_F = &(1+\alpha)\mathbf{P}_F^c - \alpha\,\mathbf{P}_F^p - \mathbf{M}_{FP}\,\ddot{\mathbf{a}}_P^c - (1+\alpha)\mathbf{C}_{FP}\,\dot{\mathbf{a}}_P^c \\ &+\alpha\left[\mathbf{C}_{FF}\,\dot{\mathbf{a}}_F^p + \mathbf{C}_{FP}\,\dot{\mathbf{a}}_P^p\right] + \alpha\,\mathbf{R}_F^p - \alpha\,\mathbf{D}_{FX}\;\mathbf{X}^p\end{aligned} \tag{12}$$

The second line of blocks is used to calculate de support reactions after solving the system of nonlinear equations given by Eq. (11).

3.2 Incremental formulation for the solution of the nonlinear dynamic equations

Since the coefficients of the vector of the internal element stresses in Eq. (10) depend on the current displacements, an iterative scheme must be adopted to obtain the solution of the equilibrium equations at the current time step. The iterative schemes most widely used for the solution of nonlinear finite element equations are based on the Newton method [13-14].

Alternatively, the nonlinear Eq. (11) can be written in the form

$$\boldsymbol{\psi}\left(\mathbf{a}_F^*, \mathbf{X}_X^*\right) = \mathbf{0} \tag{13}$$

where $\boldsymbol{\psi}$ is the vector of residual which have to be null in order to satisfy the dynamic equilibrium. For the solution $\left(\mathbf{a}_F^*, \mathbf{X}_X^*\right)$, the residual vector is given by

$$\boldsymbol{\psi}\left(\mathbf{a}_F^*, \mathbf{X}^*\right) = \overline{\mathbf{F}}_F - \mathbf{M}_{FF}\,\ddot{\mathbf{a}}_F\left(\mathbf{a}_F^*\right) - (1+\alpha)\mathbf{C}_{FF}\,\dot{\mathbf{a}}_F\left(\mathbf{a}_F^*\right) - (1+\alpha)\mathbf{R}_F\left(\mathbf{a}_F^*\right) + (1+\alpha)\,\mathbf{D}_{FX}\;\mathbf{X}^* \tag{14}$$

The nodal velocities and accelerations depend on the nodal displacements and thus are not unknowns in the equation. In the α method, the velocity and displacement at the current time step are approximated with

$$\dot{a}^c = \dot{a}^p + \left[(1-\gamma)\,\ddot{a}^p + \gamma\,\ddot{a}^c\right]\Delta t \tag{15}$$

$$a^c = a^p + \dot{a}^p\,\Delta t + \left[\left(\frac{1}{2} - \beta\right)\ddot{a}^p + \beta\,\ddot{a}^c\right]\Delta t^2 \tag{16}$$

where β and γ are parameters that control the stability and accuracy of the method. Solving Eq. (16) for $\ddot{a}^c$ gives

$$\ddot{a}^c = \frac{1}{\beta\Delta t^2}a^c - \frac{1}{\beta\Delta t^2}a^p - \frac{1}{\beta\Delta t}\dot{a}^p - \left(\frac{1}{2\beta} - 1\right)\ddot{a}^p \tag{17}$$

Substituting Eq. (17) into Eq. (15) yields

$$\dot{a}^c = \frac{\gamma}{\beta\Delta t}a^c - \frac{\gamma}{\beta\Delta t}a^p + \left(1 - \frac{\gamma}{\beta}\right)\dot{a}^p + \Delta t\left(1 - \frac{\gamma}{2\beta}\right)\ddot{a}^p \tag{18}$$

Assuming that $\mathbf{a}_F^{c,i}$ and $\mathbf{X}^{c,i}$ have already been evaluated, the function $\boldsymbol{\psi}$ can be expanded using a Taylor series [16] about the solution $\left(\mathbf{a}_F^*, \mathbf{X}^*\right)$. Neglecting the second and higher order terms leads to

$$\boldsymbol{\psi}\left(\mathbf{a}_F^*, \mathbf{X}^*\right) = \boldsymbol{\psi}\left(\mathbf{a}_F^{c,i}, \mathbf{X}^{c,i}\right) + \frac{\partial\,\boldsymbol{\psi}}{\partial\,\mathbf{a}_F^*}\left(\mathbf{a}_F^{c,i}, \mathbf{X}^{c,i}\right) \times \left(\mathbf{a}_F^* - \mathbf{a}_F^{c,i}\right) + \frac{\partial\,\boldsymbol{\psi}}{\partial\,\mathbf{X}^*}\left(\mathbf{a}_F^{c,i}, \mathbf{X}^{c,i}\right) \times \left(\mathbf{X}^* - \mathbf{X}^{c,i}\right) \tag{19}$$

where the superscript *i* denotes variables that were evaluated in the *i*th Newton iteration. Substituting Eqs. (13), (14), (17) and (18) into Eq. (19) and differentiating the function $\boldsymbol{\psi}$ with respect to the variables leads to

$$\mathbf{0} = \boldsymbol{\psi}\left(\mathbf{a}_F^{c,i}, \mathbf{X}^{c,i}\right) + \left[-\frac{1}{\beta \Delta t^2}\mathbf{M}_{FF} - (1+\alpha)\frac{\gamma}{\beta \Delta t}\mathbf{C}_{FF} - (1+\alpha)\frac{\partial \mathbf{R}_F}{\partial \mathbf{a}_F^*}\left(\mathbf{a}_F^{c,i}\right)\right]\left(\mathbf{a}_F^* - \mathbf{a}_F^{c,i}\right) + (1+\alpha)\mathbf{D}_{FX}\left(\mathbf{X}^* - \mathbf{X}^{c,i}\right) \tag{20}$$

Eq. (20) can be rearranged into the following incremental form

$$\overline{\mathbf{K}}_{FF}^{c,i}\ \Delta \mathbf{a}_F^{i+1} - (1+\alpha)\mathbf{D}_{FX}\ \Delta \mathbf{X}^{i+1} = \boldsymbol{\psi}\left(\mathbf{a}_F^{c,i}, \mathbf{X}^{c,i}\right) \tag{21}$$

where $\overline{\mathbf{K}}_{FF}^{c,i}$ is the current effective stiffness matrix defined by

$$\overline{\mathbf{K}}_{FF}^{c,i} = \frac{1}{\beta \Delta t^2}\mathbf{M}_{FF} + (1+\alpha)\frac{\gamma}{\beta \Delta t}\mathbf{C}_{FF} + (1+\alpha)\frac{\partial \mathbf{R}_F}{\partial \mathbf{a}_F^*}\left(\mathbf{a}_F^{c,i}\right) \tag{22}$$

with

$$\Delta \mathbf{a}_F^{i+1} = \mathbf{a}_F^* - \mathbf{a}_F^{c,i} \tag{23}$$

$$\Delta \mathbf{X}^{i+1} = \mathbf{X}^* - \mathbf{X}^{c,i} \tag{24}$$

Since Eq. (19) represents only a Taylor series approximation about $\left(\mathbf{a}_F^*, \mathbf{X}^*\right)$, the incremental nodal displacements and contact forces given by Eqs. (23) and (24) are used to obtain the next approximations

$$\mathbf{a}_F^{c,i+1} = \mathbf{a}_F^{c,i} + \Delta \mathbf{a}_F^{i+1} \tag{25}$$

$$\mathbf{X}^{c,i+1} = \mathbf{X}^{c,i} + \Delta \mathbf{X}^{i+1} \tag{26}$$

In matrix notation, Eq. (21) may be expressed as

$$\left[\overline{\mathbf{K}}_{FF}^{c,i} \quad \overline{\mathbf{D}}_{FX}\right]\begin{bmatrix} \Delta \mathbf{a}_F^{i+1} \\ \Delta \mathbf{X}_X^{i+1} \end{bmatrix} = \boldsymbol{\psi}\left(\mathbf{a}_F^{c,i}, \mathbf{X}^{c,i}\right) \tag{27}$$

in which

$$\overline{\mathbf{D}}_{FX} = -(1+\alpha)\mathbf{D}_{FX} \tag{28}$$

3.3 Formulation of the constraint equations

When contact occurs, a constraint equation as to be added to the system of nonlinear equations defined in Eq. (27) to avoid penetrations between the two bodies. Thus, the non-penetration condition for the normal direction is given by

$$\mathbf{v}^{CE} - \mathbf{v}^{TE} \geq -\mathbf{g} + \mathbf{r} \tag{29}$$

where $\mathbf{v}^{CE}$ are the displacements in the node of the contact element, $\mathbf{v}^{TE}$ the displacements in the auxiliary point of the target element, $\mathbf{r}$ are eventual irregularities between the contact and target elements and $\mathbf{g}$ an initial gap that separates the two elements.

The displacements of the contact nodes belonging to the contact elements are given by

$$\mathbf{v}^{CE} = \mathbf{H}_{XF}^{CE}\ \mathbf{a}_F^{c,i+1} + \mathbf{H}_{XP}^{CE}\ \mathbf{a}_P^c \tag{30}$$

where the displacement transformation matrices **H** relate the displacements of the contact nodes, defined in the local coordinate system, to the nodal displacements defined in the global coordinate system. Also, by analogy, the displacements of the auxiliary points of the target elements are given by

$$\mathbf{v}^{TE} = \mathbf{H}_{XF}^{TE}\ \mathbf{a}_F^{c,i+1} + \mathbf{H}_{XP}^{TE}\ \mathbf{a}_P^{c} \tag{31}$$

Substituting Eqs. (30) and (31) into Eq. (29) and taking into account eventual irregularities **r** between the contact and target elements yields

$$\mathbf{H}_{XF}\ \mathbf{a}_F^{c,i+1} = -\mathbf{g} + \mathbf{r} - \mathbf{H}_{XP}\ \mathbf{a}_P^{c} \tag{32}$$

where

$$\mathbf{H}_{XF} = \mathbf{H}_{XF}^{CE} - \mathbf{H}_{XF}^{TE} \tag{33}$$

$$\mathbf{H}_{XP} = \mathbf{H}_{XP}^{CE} - \mathbf{H}_{XP}^{TE} \tag{34}$$

Since only the active constraints are considered in Eq. (32) the inequality (29) becomes an equality. Substituting Eq. (25) into Eq. (32) leads to

$$\mathbf{H}_{XF}\ \Delta\mathbf{a}_F^{i+1} = -\mathbf{g} + \mathbf{r} - \mathbf{H}_{XP}\ \mathbf{a}_P^{c} - \mathbf{H}_{XF}\ \mathbf{a}_F^{c,i} \tag{35}$$

Multiplying Eq. (35) by $-(1+\alpha)$ gives

$$\overline{\mathbf{H}}_{XF}\ \Delta\mathbf{a}_F^{i+1} = \overline{\mathbf{g}} \tag{36}$$

where

$$\overline{\mathbf{H}}_{XF} = -(1+\alpha)\,\mathbf{H}_{XF} \tag{37}$$

$$\overline{\mathbf{g}} = -(1+\alpha)\left(-\mathbf{g} + \mathbf{r} - \mathbf{H}_{XP}\ \mathbf{a}_P^{c} - \mathbf{H}_{XF}\ \mathbf{a}_F^{c,i}\right) \tag{38}$$

3.4 Complete system of equations

The incremental formulation of the equilibrium equations of motion of the vehicle-structure system presented in Section 3.2 together with the contact constraint equations presented in Section 3.3 form a complete system of equations whose unknowns are incremental nodal displacements and contact forces. Eqs. (27) and (36) can be expressed in matrix form leading to the following complete system of linear equations

$$\begin{bmatrix} \overline{\mathbf{K}}_{FF}^{c,i} & \overline{\mathbf{D}}_{FX} \\ \overline{\mathbf{H}}_{XF} & \mathbf{0} \end{bmatrix} \begin{bmatrix} \Delta\mathbf{a}_F^{i+1} \\ \Delta\mathbf{X}^{i+1} \end{bmatrix} = \begin{bmatrix} \boldsymbol{\psi}\left(\mathbf{a}_F^{c,i}, \mathbf{X}^{c,i}\right) \\ \overline{\mathbf{g}} \end{bmatrix} \tag{39}$$

The symmetry of the coefficient matrix presented in Eq. (39) was demonstrated using the Betti's theorem but is not presented here due to space limitations.

The efficiency of the algorithm used for solving the system of equations (39) is very important. Thus, an efficient and stable block factorization algorithm is shown in Section 4 that takes into account the specific properties of each block, namely, symmetry, positive definiteness (if exists) and bandwidth.

4 BLOCK FACTORIZATION SOLVER ALGORTIGM

The time required to solve the system of nonlinear equations (39) represents, in the majority of the problems, the largest percentage of the total solution time. In a dynamic nonlinear analysis the effective stiffness matrix is time-dependent, which implies its factorization in each iteration. Generally, this is a major drawback since the factorization of large matrices is time consuming. However, in the present problem, the nonlinear terms are substantially smaller that the linear terms, since the material nonlinearities are concentrated only in the contact elements (Hertz contact model [5] or creep models [17]) and on nonlinear elements of the model, like vehicle suspensions or structure bearings. Hence, in order to take advantage of this situation, the effective stiffness matrix given by Eq. (22) is reordered according to the adopted d.o.f. classification presented in Section 2

$$\begin{bmatrix} \overline{\mathbf{K}}_{II}^{c,i} & \overline{\mathbf{K}}_{IR}^{c,i} & \overline{\mathbf{K}}_{IY}^{c,i} & \overline{\mathbf{D}}_{IX} \\ \overline{\mathbf{K}}_{RI}^{c,i} & \overline{\mathbf{K}}_{RR}^{c,i} & \overline{\mathbf{K}}_{RY}^{c,i} & \overline{\mathbf{D}}_{RX} \\ \overline{\mathbf{K}}_{YI}^{c,i} & \overline{\mathbf{K}}_{YR}^{c,i} & \overline{\mathbf{K}}_{YY}^{c,i} & \overline{\mathbf{D}}_{YX} \\ \overline{\mathbf{H}}_{XI} & \overline{\mathbf{H}}_{XR} & \overline{\mathbf{H}}_{XY} & \mathbf{0} \end{bmatrix} \begin{bmatrix} \Delta\mathbf{a}_I^{i+1} \\ \Delta\mathbf{a}_R^{i+1} \\ \Delta\mathbf{a}_Y^{i+1} \\ \Delta\mathbf{X}^{i+1} \end{bmatrix} = \begin{bmatrix} \boldsymbol{\psi}\left(\mathbf{a}_I^{c,i}, \mathbf{X}^{c,i}\right) \\ \boldsymbol{\psi}\left(\mathbf{a}_R^{c,i}, \mathbf{X}^{c,i}\right) \\ \boldsymbol{\psi}\left(\mathbf{a}_Y^{c,i}, \mathbf{X}^{c,i}\right) \\ \overline{\mathbf{g}} \end{bmatrix} \tag{40}$$

With this reordering, only the nonlinear terms, *R* and *Y* type d.o.f., have to be factorized in each iteration, while the largest block $\overline{\mathbf{K}}_{II}$ is factorized only once in the beginning of the dynamic analysis.

The coefficient matrix presented in Eq. (40) can be factorized as following

$$\begin{bmatrix} \overline{\mathbf{K}}_{II} & \overline{\mathbf{K}}_{IR} & \overline{\mathbf{K}}_{IY} & \overline{\mathbf{D}}_{IX} \\ \overline{\mathbf{K}}_{RI} & \overline{\mathbf{K}}_{RR} & \overline{\mathbf{K}}_{RY} & \overline{\mathbf{D}}_{RX} \\ \overline{\mathbf{K}}_{YI} & \overline{\mathbf{K}}_{YR} & \overline{\mathbf{K}}_{YY} & \overline{\mathbf{D}}_{YX} \\ \overline{\mathbf{H}}_{XI} & \overline{\mathbf{H}}_{XR} & \overline{\mathbf{H}}_{XY} & \mathbf{0} \end{bmatrix} = \begin{bmatrix} \mathbf{L}_{11} & \mathbf{0} & \mathbf{0} & \mathbf{0} \\ \mathbf{L}_{21} & \mathbf{L}_{22} & \mathbf{0} & \mathbf{0} \\ \mathbf{L}_{31} & \mathbf{L}_{32} & \mathbf{L}_{33} & \mathbf{0} \\ \mathbf{L}_{41} & \mathbf{L}_{42} & \mathbf{L}_{43} & \mathbf{L}_{44} \end{bmatrix} \times \begin{bmatrix} \mathbf{U}_{11} & \mathbf{U}_{12} & \mathbf{U}_{13} & \mathbf{U}_{14} \\ \mathbf{0} & \mathbf{U}_{22} & \mathbf{U}_{23} & \mathbf{U}_{24} \\ \mathbf{0} & \mathbf{0} & \mathbf{U}_{33} & \mathbf{U}_{34} \\ \mathbf{0} & \mathbf{0} & \mathbf{0} & \mathbf{U}_{44} \end{bmatrix} \tag{41}$$

where $\mathbf{L}_{ij}$ and $\mathbf{U}_{ij}$ are lower and upper triangle submatrices, respectively. The superscripts presented in Eq. (40) are neglected for simplification in the present section.

The first step of the solver consists on factorizing block $\overline{\mathbf{K}}_{II}$ and on calculating the upper triangle submatrix $\mathbf{U}_{12}$.

$$\overline{\mathbf{K}}_{II} = \mathbf{L}_{11}\mathbf{L}_{11}^T \tag{42}$$

$$\overline{\mathbf{K}}_{IR} = \mathbf{L}_{11}\mathbf{U}_{12} \tag{43}$$

Due to the positive-definiteness property of matrix $\overline{\mathbf{K}}_{II}$, a Cholesky factorization [18] has been used in the operation (42). Since the submatrices $\overline{\mathbf{K}}_{II}$ and $\overline{\mathbf{K}}_{IR}$ are time-independent, Eqs. (42) and (43) have to be solved only once in the beginning of the analysis.

The second step consists on calculating the remaining upper triangle submatrices. In the coefficient matrix presented in Eq. (40), the blocks $\overline{\mathbf{K}}_{RR}$ and $\overline{\mathbf{K}}_{YY}$ represent the effective stiffness matrices with the nonlinear terms, while the blocks $\overline{\mathbf{H}}_{ij}$ and $\overline{\mathbf{D}}_{ij}$ depend on the train position and on the contact status of each contact pair. Therefore, both types of blocks are time-dependent and have to be factorized in each iteration. However, the dimensions of the previous mentioned blocks are small when compared to the linear block $\overline{\mathbf{K}}_{II}$, making the next operations less expensive in terms of computational effort.

Thus, the remaining upper triangle submatrices are given by

$$\overline{\mathbf{K}}_{IY} = \mathbf{L}_{11}\,\mathbf{U}_{13} \tag{44}$$

$$\overline{\mathbf{D}}_{IX} = \mathbf{L}_{11}\,\mathbf{U}_{14} \tag{45}$$

$$\overline{\mathbf{K}}_{RR} = \mathbf{L}_{21}\,\mathbf{U}_{12} + \mathbf{L}_{22}\,\mathbf{U}_{22} \tag{46}$$

$$\overline{\mathbf{K}}_{RY} = \mathbf{L}_{21}\,\mathbf{U}_{13} + \mathbf{L}_{22}\,\mathbf{U}_{23} \tag{47}$$

$$\overline{\mathbf{D}}_{RX} = \mathbf{L}_{21}\,\mathbf{U}_{14} + \mathbf{L}_{22}\,\mathbf{U}_{24} \tag{48}$$

As mentioned before, the nonlinear contact elements make the connection between the two systems, vehicle and structure. Depending of the problem, the stiffness matrix of these elements can assume other properties other than positive definiteness, thus it cannot be solved with factorization methods without pivoting, like Cholesky or $\mathbf{L}\mathbf{D}\mathbf{L}^T$ [18]. Therefore, the proposed block factorization algorithm evaluates the positive definiteness of the block $\overline{\mathbf{K}}_{YY}$ and solves it with pivoting if needed, as explained below.

The third part of the solver consists on solving the following intermediate system of equations

$$\begin{bmatrix} \mathbf{L}_{11} & \mathbf{0} & \mathbf{0} & \mathbf{0} \\ \mathbf{L}_{21} & \mathbf{L}_{22} & \mathbf{0} & \mathbf{0} \\ \mathbf{L}_{31} & \mathbf{L}_{32} & \mathbf{L}_{33} & \mathbf{0} \\ \mathbf{L}_{41} & \mathbf{L}_{42} & \mathbf{L}_{43} & \mathbf{L}_{44} \end{bmatrix} \begin{bmatrix} \mathbf{y}_1 \\ \mathbf{y}_2 \\ \mathbf{y}_3 \\ \mathbf{y}_4 \end{bmatrix} = \begin{bmatrix} \boldsymbol{\psi}(\mathbf{a}_I, \mathbf{X}) \\ \boldsymbol{\psi}(\mathbf{a}_R, \mathbf{X}) \\ \boldsymbol{\psi}(\mathbf{a}_Y, \mathbf{X}) \\ \overline{\mathbf{g}} \end{bmatrix} \tag{49}$$

in which the vectors $\mathbf{y}_1$ to $\mathbf{y}_4$ are obtained by forward substitution

$$\mathbf{L}_{11}\,\mathbf{y}_1 = \boldsymbol{\psi}(\mathbf{a}_I, \mathbf{X}) \tag{50}$$

$$\mathbf{L}_{22}\,\mathbf{y}_2 = \boldsymbol{\psi}(\mathbf{a}_R, \mathbf{X}) - \mathbf{L}_{21}\,\mathbf{y}_1 \tag{51}$$

$$\overline{\mathbf{y}}_3 = \mathbf{L}_{33}\,\mathbf{y}_3 \tag{52}$$

$$\overline{\mathbf{y}}_4 = \mathbf{L}_{43}\,\mathbf{y}_3 + \mathbf{L}_{44}\,\mathbf{y}_4 \tag{53}$$

where

$$\overline{\mathbf{y}}_3 = \boldsymbol{\psi}(\mathbf{a}_Y, \mathbf{X}) - \mathbf{L}_{31}\,\mathbf{y}_1 - \mathbf{L}_{32}\,\mathbf{y}_2 \tag{54}$$

$$\overline{\mathbf{y}}_4 = \overline{\mathbf{g}} - \mathbf{L}_{41}\,\mathbf{y}_1 - \mathbf{L}_{42}\,\mathbf{y}_2 \tag{55}$$

Finally, the solution of the system equations is given by

$$\begin{bmatrix} \mathbf{U}_{11} & \mathbf{U}_{12} & \mathbf{U}_{13} & \mathbf{U}_{14} \\ \mathbf{0} & \mathbf{U}_{22} & \mathbf{U}_{23} & \mathbf{U}_{24} \\ \mathbf{0} & \mathbf{0} & \overline{\mathbf{A}}_{33} & \overline{\mathbf{A}}_{43}^T \\ \mathbf{0} & \mathbf{0} & \overline{\mathbf{A}}_{43} & \overline{\mathbf{A}}_{44} \end{bmatrix} \begin{bmatrix} \Delta\mathbf{a}_I \\ \Delta\mathbf{a}_R \\ \Delta\mathbf{a}_Y \\ \Delta\mathbf{X} \end{bmatrix} = \begin{bmatrix} \mathbf{y}_1 \\ \mathbf{y}_2 \\ \overline{\mathbf{y}}_3 \\ \overline{\mathbf{y}}_4 \end{bmatrix} \tag{56}$$

where the first part of the solution of the system, $\Delta\mathbf{a}_Y$ and $\Delta\mathbf{X}$, is obtained by factorizing and solving the two last lines of blocks with pivoting

$$\begin{bmatrix} \overline{\mathbf{A}}_{33} & \overline{\mathbf{A}}_{43}^{T} \\ \overline{\mathbf{A}}_{43} & \overline{\mathbf{A}}_{44} \end{bmatrix} \begin{bmatrix} \Delta\mathbf{a}_Y \\ \Delta\mathbf{X} \end{bmatrix} = \begin{bmatrix} \overline{\mathbf{y}}_3 \\ \overline{\mathbf{y}}_4 \end{bmatrix} \tag{57}$$

in which

$$\overline{\mathbf{A}}_{33} = \overline{\mathbf{K}}_{YY} - \mathbf{L}_{31}\mathbf{L}_{31}^{T} - \mathbf{L}_{32}\mathbf{L}_{32}^{T} \tag{58}$$

$$\overline{\mathbf{A}}_{43} = \overline{\mathbf{H}}_{XY} - \mathbf{L}_{41}\mathbf{L}_{31}^{T} - \mathbf{L}_{42}\mathbf{L}_{32}^{T} \tag{59}$$

$$\overline{\mathbf{A}}_{44} = -\mathbf{L}_{41}\mathbf{L}_{41}^{T} - \mathbf{L}_{42}\mathbf{L}_{42}^{T} \tag{60}$$

and the last part of the solution, $\Delta\mathbf{a}_I$ and $\Delta\mathbf{a}_R$, is obtained by back substitution

$$\mathbf{L}_{22}^{T}\Delta\mathbf{a}_R = \mathbf{y}_2 - \mathbf{L}_{32}^{T}\Delta\mathbf{a}_Y - \mathbf{L}_{42}^{T}\Delta\mathbf{X} \tag{61}$$

$$\mathbf{L}_{11}^{T}\Delta\mathbf{a}_I = \mathbf{y}_1 - \mathbf{L}_{21}^{T}\Delta\mathbf{a}_R - \mathbf{L}_{31}^{T}\Delta\mathbf{a}_Y - \mathbf{L}_{41}^{T}\Delta\mathbf{X} \tag{62}$$

5 NUMERICAL VALIDATION

In order to validate the accuracy of the proposed methodology a numeric examples is presented in this section. The example consists of two simply supported spans subjected to four moving sprung masses (see Figure 3). The spans are modeled with solid elements in order to test not only the accuracy, but also the efficiency of the algorithm. The two simply supported spans are discretized with sixteen thousand 8-node solid elements ($2\times80\times10\times10$) and have a total of 58696 unconstrained d.o.f. The geometrical and mechanical properties of the system are the following: length of each span $L = 20\,\text{m}$, width of the square cross section b = 2.45 m, Young's modulus $E = 25\,\text{GPa}$, Poisson's ratio $\nu = 0.2$, moment of inertia $I = 3\,\text{m}^4$, mass per unit length $m = 30000\ \text{kg/m}$, suspended mass $M_v = 30000\,\text{kg}$ and spring stiffness $k_v = 156550\ \text{kN/m}$. The distance between each sprung mass is $d = 20\,\text{m}$.

The results obtained using the direct method are compared with the results obtained by the commercial software ANSYS [12], using the Lagrange multiplier method [5].

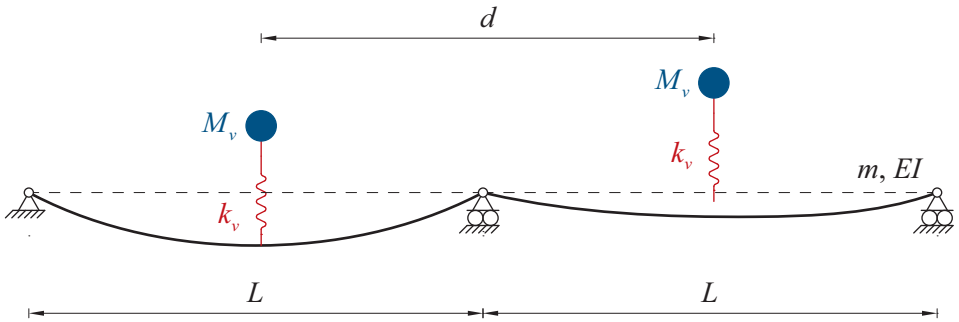

Figure 3: Two simply supported spans subjected to four moving sprung masses.

The sprung masses move at a constant speed $\text{v} = 115\,\text{m/s}$. The following parameters for the α method are considered: $\alpha = 0$, $\beta = 0.25$ and $\gamma = 0.5$, which correspond to the constant average acceleration method. The time step is $\Delta t = 0.001\text{s}$ and the total number of time steps is 900.

The vertical displacement at the midpoint of the first span, obtained using the direct method and ANSYS, is plotted in Figure 4. The vertical displacements of the first and last sprung masses, SM1 and SM4 respectively, are compared in Figure 5. The results obtained using the proposed methodology and ANSYS show a very good agreement.

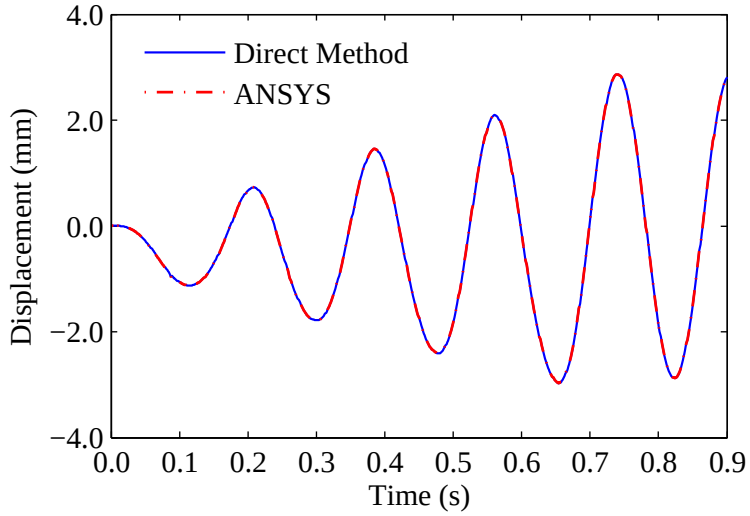

Figure 4: Vertical displacement at the midpoint of the first span.

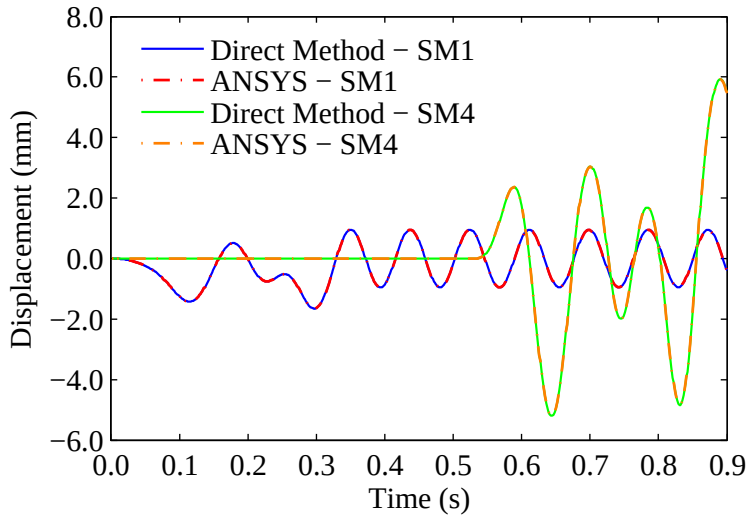

Figure 5: Vertical displacement of the first and last suspended masses.

Finally, the comparisons between the contact forces of the first and last sprung masses are plotted in Figure 6. The results obtained using the direct method perfectly match the corresponding ANSYS solutions obtained using the well-known Lagrange multiplier method. As was expected, the first sprung mass is in permanent contact during all the analysis, since the excitation of the beam is not enough to cause the sprung mass separation. However, the last sprung mass loses contact with the beam a significant number of times as can be observed in Figure 6 when the contact force is zero. This is due to the fact that the excitation of the beam is considerably higher during the passage of the last sprung mass. Therefore, the present methodology demonstrates good accuracy both when the vehicle detaches from the structure and when reattaches.

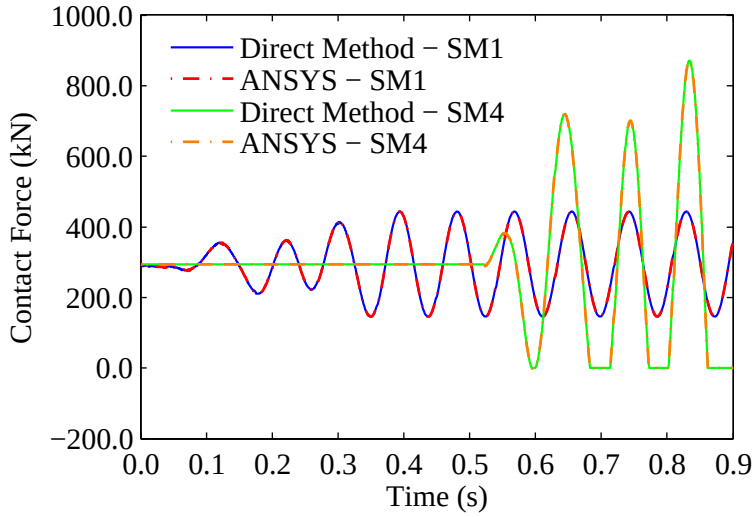

Figure 6: Vertical contact force of the first and last suspended masses.

The calculations of the present example were performed using a workstation with an Intel Xeon E5620 dual core processor running at 2.40 GHz. For a more accurate comparison the calculations in ANSYS and MATLAB were performed using a single thread. The execution time was 16608 seconds using ANSYS and 264 seconds using the direct method with the optimized block factorization algorithm, which is about 63 times faster. Hence, in terms of computational speed, the direct method has proven to be very efficient.

6 CONCLUSIONS

An accurate and efficient methodology for analyzing the vehicle-structure interaction problem has been developed. The nonlinear equations of motion of the vehicle and structure are complemented with additional constraint equations, forming a single system of equations that can be directly and efficiently solved. Due to the nonlinear nature of the contact mechanics, an incremental formulation has been used to solve the equations of motion, while a procedure based on the Lagrange multiplier method imposes the contact constraint equations when contact occurs. The system of nonlinear equations is solved by block factorization solver that reorders the system matrix and isolates the nonlinear terms, thus avoiding multiple unnecessary factorizations of the linear terms during each Newton iteration.

The accuracy and efficiency of the proposed methodology has been confirmed with a numerical example. The example consisted of two simply supported spans modeled with 8-node solid elements subjected to four moving sprung masses, totalizing 58684 unconstrained d.o.f. The responses of the structure, vehicles as well as the contact forces obtained with the proposed methodology have been compared with the results obtained with the commercial software ANSYS using the Lagrange multiplier method. A good agreement between the proposed methodology and ANSYS has been observed. In terms of efficiency, the proposed methodology has also showed very good results, since it is about 63 times faster than ANSYS.

ACKNOWLEDGMENTS

The authors wish to thank Professor Rui Manuel Faria of the University of Porto for the helpful discussions during the preparation of this manuscript, especially regarding the incremental formulation used in this work. This article reports research developed under financial support provided by "FCT - Fundação para a Ciência e Tecnologia", Portugal, under grant number SFRH/BD/39190/2007 and SFRH/BD/48320/2008.

REFERENCES

[1] Delgado, R., Santos, S.M. - Modelling of railway bridge-vehicle interaction on high speed tracks, *Computers & Structures*, **63**, 511-523, 1997.

[2] Lei, X., Noda, N.A. - Analyses of dynamic response of vehicle and track coupling system with random irregularity of track vertical profile, *Journal of Sound and Vibration*, **258**, 147-165, 2002.

[3] Yang, F., Fonder, G. - An iterative solution method for dynamic response of bridge-vehicles systems, *Earthquake Engineering and Structural Dynamics*, **25**, 195-215, 1996.

[4] Yang, Y.B., Wu, Y.S. - A versatile element for analyzing vehicle-bridge interaction response, *Engineering Structures*, **23**, 452-469, 2001.

[5] Wriggers, P. - *Computational Contact Mechanics*, John Wiley & Sons Ltd, Chichester, UK, 2002.

[6] Pombo, J., Ambrosio, J., Silva, M. - A new wheel-rail contact model for railway dynamics, *Vehicle System Dynamics*, **45**, 165-189, 2007.

[7] Shabana, A., Zaazaa, K.E., Escalona, J.L., Sany, J.R. - Development of elastic force model for wheel/rail contact problems, *Journal of Sound and Vibration*, **269**, 295-325, 2004.

[8] Antolín, P., Goicolea, J.M., Oliva, J., Astiz, M.A. - Nonlinear train-bridge lateral interaction using a simplified wheel-rail contact method within a finite element framework, *Journal of Computational and Nonlinear Dynamics*, **7**, art. no. 041014, 2012.

[9] Tanabe, M., Matsumoto, N., Wakui, H., Sogabe, M., Okuda, H., Tanabe, Y. - A simple and efficient numerical method for dynamic interaction analysis of a high-speed train and railway structure during an earthquake, *Journal of Computational and Nonlinear Dynamics*, **3**, art. no. 041002, 2008.

[10] Neves, S.G.M., Azevedo, A.F.M., Calçada, R. - A direct method for analyzing the vertical vehicle–structure interaction, *Engineering Structures*, **34**, 414-420, 2012.

[11] MATLAB® - R2011b, The MathWorks Inc., Natick, MA, 2011.

[12] ANSYS® - Academic Research, Release 13.0, ANSYS Inc., Canonsburg, PA, 2010.

[13] Bathe, K.J. - *Finite element procedures*, Upper Saddle River, NJ: Prentice-Hall, 1996.

[14] Owen, D.R.J., Hinton, E. - *Finite Elements in Plasticity: Theory and Practice*, Swansea, UK: Pineridge Press Limited, 1980.

[15] Hughes, T.J.R. - *The finite element method: Linear static and dynamic finite element analysis*, Dover Publications, New York, 2000.

[16] Arfken, G. - *Mathematical methods for physicists*, Orlando, FL: Academic Press, 1985.

[17] Kalker, J.J. - *Three-dimensional elastic bodies in rolling contact*, Kluwer Academic Publishers, Dordrecht, The Netherlands, 1990.

[18] Burden, R.L., Faires, J.D. - *Numerical analysis*, ITP, Pacific Grove, CA, 1997.